

# Electrochemical Immunosensor for Monocyte Chemoattractant Protein-1 Detection Based on Pt Nanoparticles Functionalized Single-walled Carbon Nanohorns

Zhengshan Gao, Xiang Liu, Chengli Zhang, Zhiyong Tang, Jun Chen, Chao Yu\*

College of Pharmacy, and Chongqing pharmacodynamic evaluation engineering technology research center, Chongqing Medical University, Chongqing 400016, P.R. China

\*E-mail: [yuchaom@163.com](mailto:yuchaom@163.com)

Received: 24 December 2017 / Accepted: 6 February 2018 / Published: 6 March 2018

---

A novel label-free electrochemical sensing strategy for detecting monocyte chemoattractant protein-1 (MCP-1) was developed by using single-walled carbon nanohorns (SWCNHs) functionalized with Pt nanoparticles (PtNPs-SWCNHs). After modification with the PtNPs-SWCNHs, the electrode could serve as an effective platform for antibody immobilization and electron transfer owing to the large surface area and excellent conductivity of PtNPs-SWCNHs. Moreover, the PtNPs-SWCNHs composite could provide an obvious electrochemical signal through amperometric *i-t* curve method, due to its high catalytic activity for the reduction of hydrogen peroxide (H<sub>2</sub>O<sub>2</sub>). Under optimal conditions, the amperometric *i-t* curve signals had a strong linear relation with the logarithm of the MCP-1 concentration ranging from 0.06 pg mL<sup>-1</sup> to 450 pg mL<sup>-1</sup>, and the detection limit was 0.02 pg mL<sup>-1</sup>. Furthermore, the proposed immunosensor could detect MCP-1 in serum samples with desirable results. Overall, this immunosensor may provide a new alternative strategy for rapid detection of MCP-1.

---

**Keywords:** Monocyte chemoattractant protein-1; Single-walled carbon nanohorns; Pt nanoparticles; Electrochemical immunosensor.

## 1. INTRODUCTION

Atherosclerosis is recognized as a progressive inflammatory disease, and the overexpression of inflammatory cytokines is thought to be an important event that occurs in every phase of its development [1]. Monocyte chemoattractant protein-1 (MCP-1), as a pivotal inflammatory cytokine, plays an important role in the development of atherosclerosis [2]. MCP-1 is a member of the C-C subfamily of chemokines, which can also be referred to as C-C motif chemokine ligand 2 (CCL2) [3]. In the early stage of atherosclerosis, MCP-1 promotes atherosclerosis by recruiting macrophages and

monocytes to the vessel wall [4]. According to previous research, the upregulated expression of MCP-1 could be found in the atherosclerotic lesions [5]. Since the MCP-1 plasma level is associated with the early stage of atherogenesis, MCP-1 has the potential to serve as a biomarker of atherosclerosis [6]. Thus, developing a convenient, sensitive and highly specific method for the detection of MCP-1 is an important subject.

In recent years, electrochemical immunosensors have been extensively used in the detection of clinical samples and have attracted great interest due to their features of rapid detection, high sensitivity and excellent specificity [7]. In particular, label-free immunosensors have attracted significant attention because they have simplified assembling processes and provided an efficient method to detect biomarkers [8]. To date, nanomaterials with unique structural features and catalytic properties have been successfully utilized for the construction of electrochemical immunosensors, including metallic nanoparticles, carbon nanotubes, carbon nanofibers, graphene and nanocomposites [9-13].

Single-walled carbon nanohorns (SWCNHs), as a type of carbon materials, are spherical aggregates of horn-shaped single-walled tubules [14]. Compared with traditional carbon nanomaterials, the unique structural features of SWCNHs make them have many superior properties, such as excellent conductivity, high porosity, high purity, good biocompatibility and low toxicity [15]. On account of their superior physicochemical characteristics, SWCNHs are considered as promising materials for drug delivery, gas storage, fuel cells, biosensors, etc [16-19]. Recently, some research has been done to explore their potential applications in electrochemical analysis. For instance, F. Valentini developed an ultrasensitive electrochemical sensor for detecting epinephrine by using oxidized SWCNHs (oxSWCNHs) to modify screen-printed electrodes [20]. It is well known that noble metal nanoparticles have broad applications in the fabrication of immunosensors [21-24]. Among them, Pt nanoparticles possess excellent conductivity and feature efficient biomolecule immobilization [25-26]. In particular, Pt nanoparticles could provide an obvious electrochemical signal through amperometric *i*-*t* curve method due to their high catalytic activity for the catalytic reduction of hydrogen peroxide (H<sub>2</sub>O<sub>2</sub>) [27]. In this work, we modified pristine SWCNHs with Pt nanoparticles. Pt nanoparticles functionalized SWCNHs (PtNPs-SWCNHs) are a new functionalized material that simultaneously possesses the unique properties of SWCNHs and Pt nanoparticles. In addition, due to the unique structure of SWCNHs, the durability of Pt nanoparticles would be improved [28]. The resulting nanocomposite has excellent electrochemical properties, which could tremendously improve the sensitivity and stability of the electrochemical immunosensor.

In this work, a rapid and convenient electrochemical sensor for the detection of MCP-1 was fabricated using PtNPs-SWCNHs coupled with a glassy carbon electrode (GCE). To the best of our knowledge, this label-free electrochemical sensing strategy was first reported. PtNPs-SWCNHs were synthesized in an aqueous solution at room temperature through a one-step reaction. Superior electrochemical performances were achieved after the electrode was modified with the PtNPs-SWCNHs. Then, a sensitive immunosensor was finished by further assembling MCP-1 on the electrode surface. The proposed immunosensor has three noticeable advantages: (1) the synthetic method of PtNPs-SWCNHs is simple and feasible, (2) the fabrication process of this immunosensor is convenient, and the immunosensor offers rapid detection of MCP-1, (3) this electrochemical

sensing strategy has a wide linear range (from 0,06 to 450 pg mL<sup>-1</sup>) and a low detection limit (0.02 pg mL<sup>-1</sup>). Moreover, this immunosensor could be applied for the analysis of serum samples with good recoveries. Hence, this immunosensing method could provide potential applications for the ultrasensitive detection of MCP-1.

## 2. EXPERIMENTAL

### 2.1 Materials and Reagents

SWCNHs (>97% purity) were purchased from Nanjing XFNANO Materials Tech Co., Ltd. (China). Chloroplatinic acid (H<sub>2</sub>PtCl<sub>6</sub>) and uric acid (UA) were obtained from Sigma-Aldrich (St. Louis, USA, [www.sigmaaldrich.com](http://www.sigmaaldrich.com)). NaBH<sub>4</sub> and H<sub>2</sub>O<sub>2</sub> were brought from Chongqing Chuandong Chemical Group Co., Ltd (Chongqing, China). Potassium ferricyanide (K<sub>3</sub>Fe(CN)<sub>6</sub>), potassium ferrocyanide (K<sub>4</sub>Fe(CN)<sub>6</sub>) and bovine serum albumin (BSA) were supplied from Beijing Chemical Reagents Company (Beijing, China). Phosphate buffered saline (PBS) (pH 7.4, 0.1 M) which was prepared with Na<sub>2</sub>HPO<sub>4</sub> and KH<sub>2</sub>PO<sub>4</sub>. Ascorbic acid (AA), glucose (Glu) and L-cysteine (L-Cys) were obtained from Aladdin (China, [www.aladdin-e.com](http://www.aladdin-e.com)). Clinical serum samples were provided by the First Affiliated Hospital of Chongqing Medical University (Chongqing, China). All other reagents were analytical grade and were used as received without further purification. All aqueous solutions were prepared with ultrapure water (>18.2 MΩ) supplied by a Millipore Milli-Q purification system.

### 2.2 Apparatus

Field emission scanning electron microscopy (FE-SEM) observations were conducted on a Hitachi S4800 (Hitachi Limited, Japan) system. The transmission electron microscope (TEM) images were obtained using a Hitachi-7500158 scanning electron microscope (Japan). X-ray photoelectron spectroscopy (XPS) measurements were performed using a VG Scientific ESCALAB 250 spectrometer (Thermoelectricity Instruments, USA) with an Al Kα X-ray (1486.6 eV) as the light source. Energy dispersive X-ray spectroscopy (EDS) was conducted on a JEOL JSM-6700F microscope (Japan, [www.jeol.co.jp](http://www.jeol.co.jp)). Atomic force microscopy (AFM) measurements were made using a Bruker Dimension icon (USA) instrument. All electrochemical experiments were performed on a CHI660E electrochemical workstation (Chenhua Instruments Co., Shanghai, China, [instrument.cn.gongchang.com](http://instrument.cn.gongchang.com)) with a platinum auxiliary electrode, saturated calomel reference electrode and modified glassy carbon working electrode.

### 2.3 Preparation of the PtNPs-SWCNHs nanocomposite

The PtNPs-SWCNHs were prepared as follows. First, 1 mg of the SWCNHs was dispersed in 1 mL of ultrapure water and sonicated for 2 h to obtain a homogeneous aqueous solution. Then, 2 mL of 0.5% H<sub>2</sub>PtCl<sub>6</sub> was added to the above solution and followed by sonicating and stirring for 4 h to ensure

that the negatively charged  $\text{PtCl}_6^{2-}$  ions adequately adsorbed onto the surfaces of the SWCNHs. Next, 10 mL of a 0.01 M ice-cold  $\text{NaBH}_4$  solution was added dropwise into the mixture solution with stirring. The mixture was continually stirred for 2 h. In the end, the PtNPs-SWCNHs were collected by centrifugation and washing for several cycles. The products were stored at 4 °C.

#### 2.4 Fabrication of the biosensor

The glassy carbon electrode (GCE) was consecutively polished to a mirror-like surface with 0.3 and 0.05  $\mu\text{m}$  alumina slurries, followed by successive sonication with ethanol and ultrapure water. Then, 8  $\mu\text{L}$  of the prepared PtNPs-SWCNHs nanocomposite solution was dropped on the electrode surface and dried in air. Next, 8  $\mu\text{L}$  of the anti-MCP-1 solution was added onto the electrode surface to incubate for 12 h at 4 °C. Afterwards, the electrode was rinsed with double-distilled water to remove excess antibodies. To block possible non-specific binding sites, the obtained electrode was incubated with 6  $\mu\text{L}$  of BSA (1 wt%) for 30 min at 37 °C. Finally, the redundant BSA on the electrode was washed with ultrapure water, and the finished biosensor was stored at 4 °C until electrochemical measurements. The fabrication process of the immunosensor is illustrated in Fig. 1.

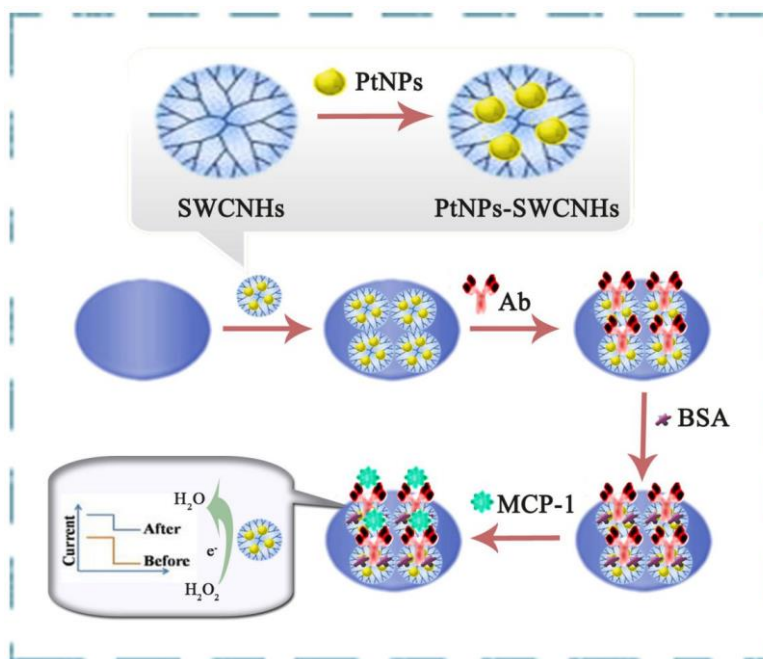


**Figure 1.** Schematic of the fabrication of an electrochemical platform for MCP-1 detection based on PtNPs-SWCNHs.

#### 2.5 Experimental measurements

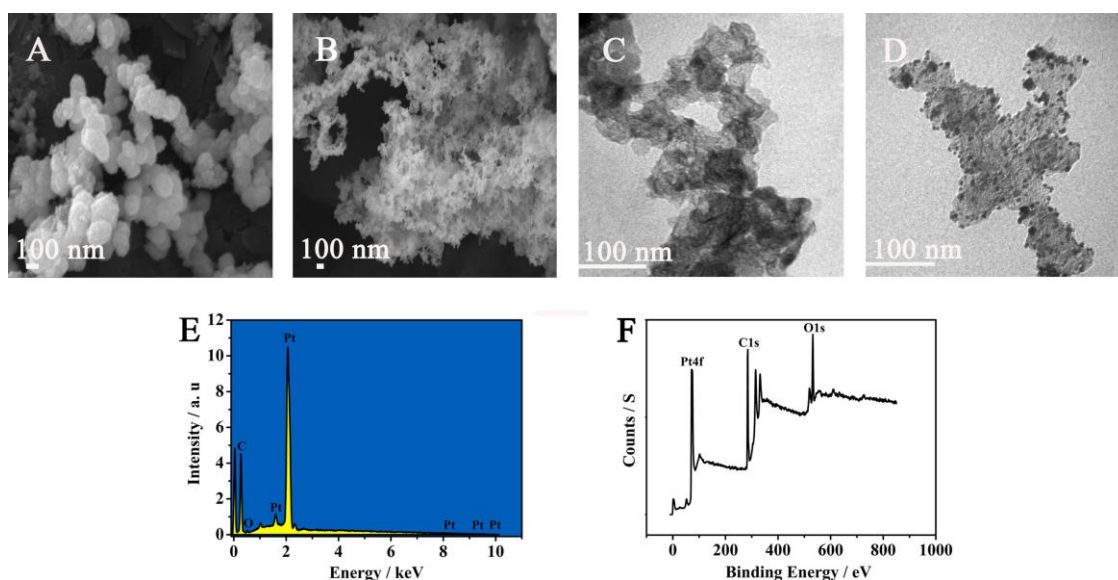
Before the electrochemical measurements, the fabricated biosensors were incubated with 6  $\mu\text{L}$  of different concentrations of MCP-1 for 60 min, followed by washing with ultrapure water.

Ultimately, amperometric  $i-t$  curve was performed at  $-0.4$  V in 5 mL of PBS ( $\text{pH}=7.4$ ), with the participation of an appropriate quantity of  $\text{H}_2\text{O}_2$  as the substrate.

### 3. RESULTS AND DISCUSSION

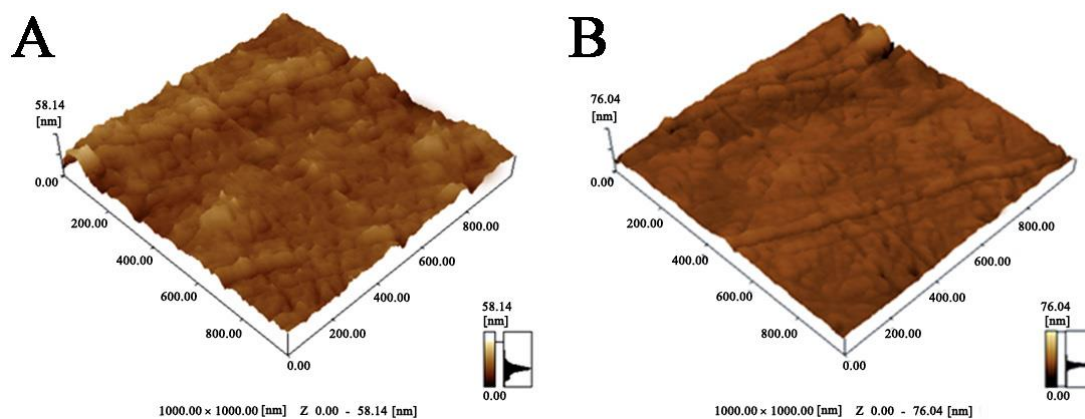
#### 3.1 Characterization of the nanomaterials

Fig. 2A-B illustrates the SEM images of the pristine SWCNHs and the PtNPs-SWCNHs composite. As revealed in Fig. 2A, pristine SWCNHs have a spherical nanostructure which is consistent with the previous report [29]. Fig. 2B clearly shows that plenty of Pt nanoparticles are dispersed uniformly on the surfaces of the pristine SWCNHs, which increases the surface area [30]. Fig. 2C-D provides TEM images of the same samples. As shown in Fig. 2C, SWCNHs exhibit a typical morphology of dahlia bundles [31]. According to Fig. 2D, the structure of the SWCNHs was not destroyed after depositing the Pt nanoparticles, which afforded superior electrochemical properties for the fabrication of electrochemical biosensors [30]. Energy dispersive spectrometer (EDS) analyses (Fig. 2E) confirmed the coexistence of C and Pt, which proved that the Pt-SWCNHs were successfully synthesized. Furthermore, X-ray photoelectron spectroscopy (XPS) was used to characterize the surface composition of the PtNPs-SWCNHs (Fig. 2F). As expected, the Pt4f peak was obtained at 72.58 eV, which demonstrated the presence of Pt nanoparticles. The peaks of C1s and O1s were observed at 284.84 eV and 532.09 eV, respectively. Thus, the results of XPS also proved the existence of Pt nanoparticles on the surface of the SWCNHs. All data showed that the PtNPs-SWCNHs nanocomposite was successfully prepared.



**Figure 2.** SEM images of (A) SWCNHs and (B) PtNPs-SWCNHs. TEM images of (C) SWCNHs and (D) PtNPs-SWCNHs. (E) EDS spectrum of PtNPs-SWCNHs. (F) XPS spectrum of PtNPs-SWCNHs.

Moreover, the bioconjugation between anti-MCP-1 and the PtNPs-SWCNHs was investigated by atomic force microscopy (AFM). AFM images of PtNPs-SWCNHs treated without and with anti-MCP-1 are shown in Fig. 3A and Fig. 3B, respectively. The PtNPs-SWCNHs modified electrode had a homogenous and dense surface. The average roughness of this surface was 7.653 nm on a  $1 \times 1 \mu\text{m}$  scale. After the immobilization of anti-MCP-1, the electrode surface was smoother. An average roughness value of 6.164 nm on a  $1 \times 1 \mu\text{m}$  scale was achieved. This decrease was because antibody molecules filled the surface cracks of the nanocomposites [32]. The results of the AFM studies indicated anti-MCP-1 had been successfully immobilized on the electrode surface.



**Figure 3.** AFM images of (A) PtNPs-SWCNHs and (B) anti-MCP-1 / PtNPs-SWCNHs.

### 3.2 Characterization of the immunosensor

Cyclic voltammetry (CV) was utilized to investigate the fabrication process of the immunosensor. As shown in Fig. 4A, the bare GCE exhibited a pair of reversible redox peaks in the classical  $\text{Fe}(\text{CN})_6^{3-/4-}$  system (curve a). After modification with PtNPs-SWCNHs, the peak current increased dramatically owing to the good conductivity of the PtNPs-SWCNHs (curve b) [33]. Then, after the successive immobilization of anti-MCP-1, BSA and MCP-1 on the electrode, the redox peak current decreased gradually (curve c, d and e), which was attributed to the fact that these proteins with poor conductivity hindered the interfacial electron transfer [34]. The CV characterization revealed the immunosensor was successfully prepared.

CV results were further confirmed via amperometric  $i-t$  curve, which is an effective method for studying the catalytic performance of the electrode surface (Fig. 4B) [35]. Specifically, bare GCE showed an almost straight line (curve a). After the deposition of the PtNPs-SWCNs, a very obvious electrocatalytic current response was observed (curve b), which was attributed to the high catalytic activity of the nanocomposites. When the electrode was modified with anti-MCP-1, the electrocatalytic current response notably decreased due to the non-conductive character of the bioactive substances. For the same reason, the electrocatalytic current response continued to decrease when the electrode was modified with BSA and MCP-1 (curve d and e). The above experimental phenomena corresponded with the results of the CV test, which further proved the immunosensor was successfully finished.

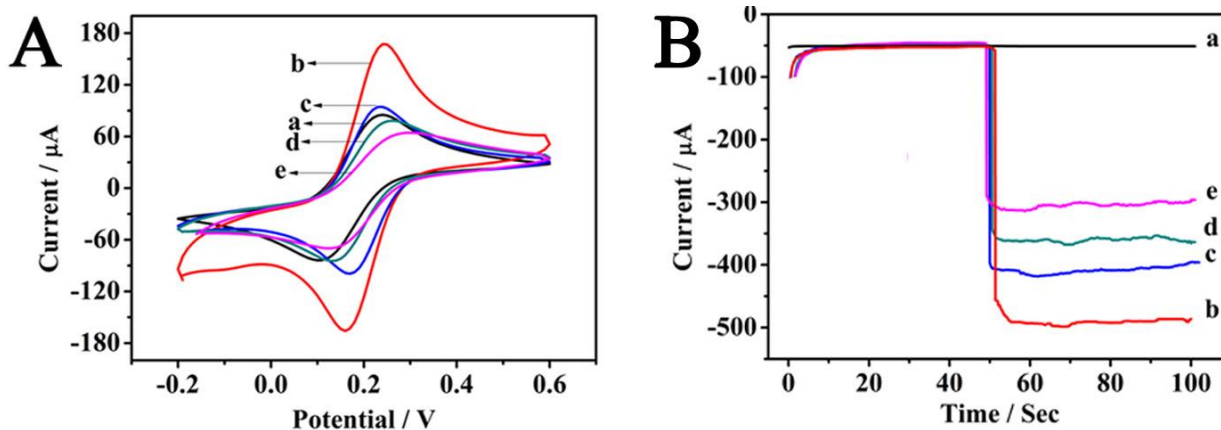


**Figure 4.** (A) CV performance in a 5 mM  $\text{Fe}(\text{CN})_6^{3-/4-}$  solution; (B) Amperometric i-t curve responses towards  $\text{H}_2\text{O}_2$  in PBS at pH = 7.4. (a) GCE; (b) PtNPs-SWCNHs / GCE; (c) anti-MCP-1 / PtNPs-SWCNHs / GCE; (d) BSA / anti-MCP-1 / Pt-SWCNHs / GCE; (e) MCP-1 / BSA / anti-MCP-1 / PtNPs-SWCNHs / GCE.

### 3.3 Optimization of the experimental conditions

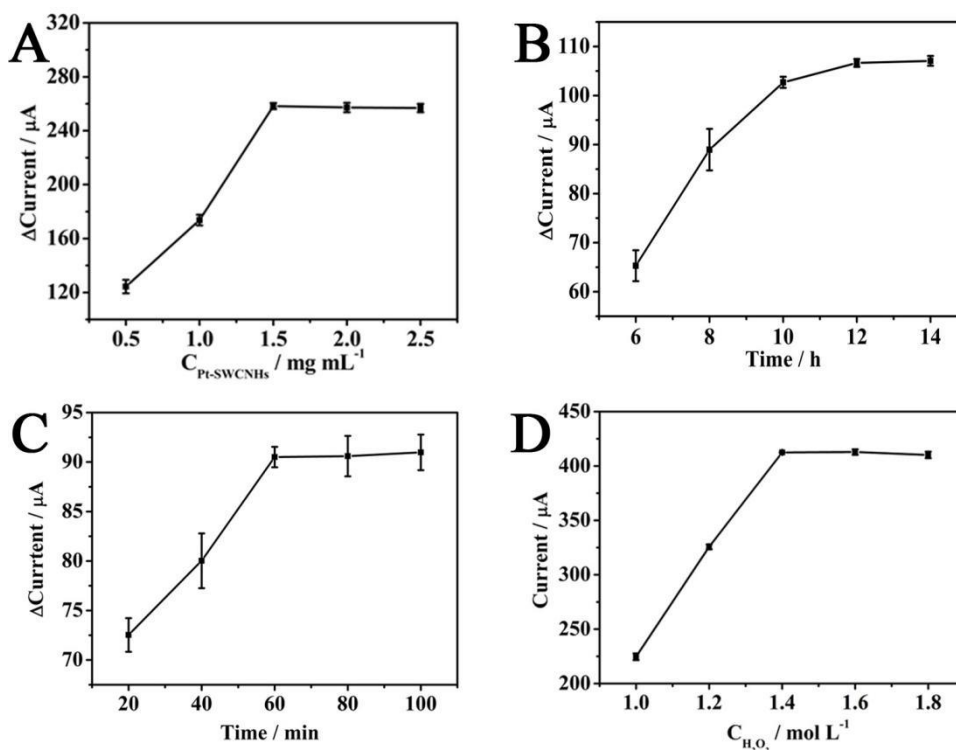


**Figure 5.** Effects of the (A) concentration of the PtNPs-SWCNHs, (B) incubation time of the anti-MCP-1, (C) incubation time between the anti-MCP-1 and MCP-1, and the (D) concentration of  $\text{H}_2\text{O}_2$ .

To obtain an excellent analytical performance for MCP-1, the experimental conditions were optimized (Fig. 5). The concentration of the PtNPs-SWCNHs is a major factor affecting the response

of the immunosensor. With an increasing concentration of PtNPs-SWCNHs, the current response increased sharply and reached a maximum value at  $1.5 \text{ mg mL}^{-1}$  (Fig. 5A). Therefore,  $1.5 \text{ mg mL}^{-1}$  was employed as the performed concentration in subsequent experiments. The electrochemical signal is also related to the incubation time of the anti-MCP-1. Obviously, a maximum difference of the current response was observed when the incubation time was 12 h, and this did not change obviously after 12 h (Fig. 5B). Thus, we chose 12 h as the optimal incubation time for the detection of anti-MCP-1. Similarly, 60 min was selected as the incubation time between the anti-MCP-1 and MCP-1 (Fig. 5C). Furthermore, the concentrations of  $\text{H}_2\text{O}_2$  were evaluated from  $1.0 \text{ mol L}^{-1}$  to  $1.8 \text{ mol L}^{-1}$ . With the increase of  $\text{H}_2\text{O}_2$ , the current response increased gradually, and the maximum response was obtained when the  $\text{H}_2\text{O}_2$  concentration reached  $1.4 \text{ mol L}^{-1}$  (Fig. 5D). Hence,  $1.4 \text{ mol L}^{-1}$  was chosen as the optimal concentration in this work.

### 3.4 Analytical performance of the immunosensor

The analytical performance of the fabricated immunosensor was explored by measuring the standard MCP-1 solution with different concentrations under optimal conditions. As the concentration of MCP-1 increased, the electrocatalytic current response decreased accordingly because the catalytic reaction was retarded by MCP-1 (Fig. 6A). We received a linear regression equation:  $Y = 53.43 + 21.10 \log C_{\text{MCP-1}}$  ( $R^2 = 0.9959$ ,  $0.06 \sim 450 \text{ pg mL}^{-1}$ ) (Fig. 6B). The detection limit was calculated to be  $0.02 \text{ pg mL}^{-1}$  ( $S/N = 3$ ). Furthermore, the comparison of this method with other works related to MCP-1 detection is shown in Table 1. Clearly, the detection limit of this method is superior to other reported methods.

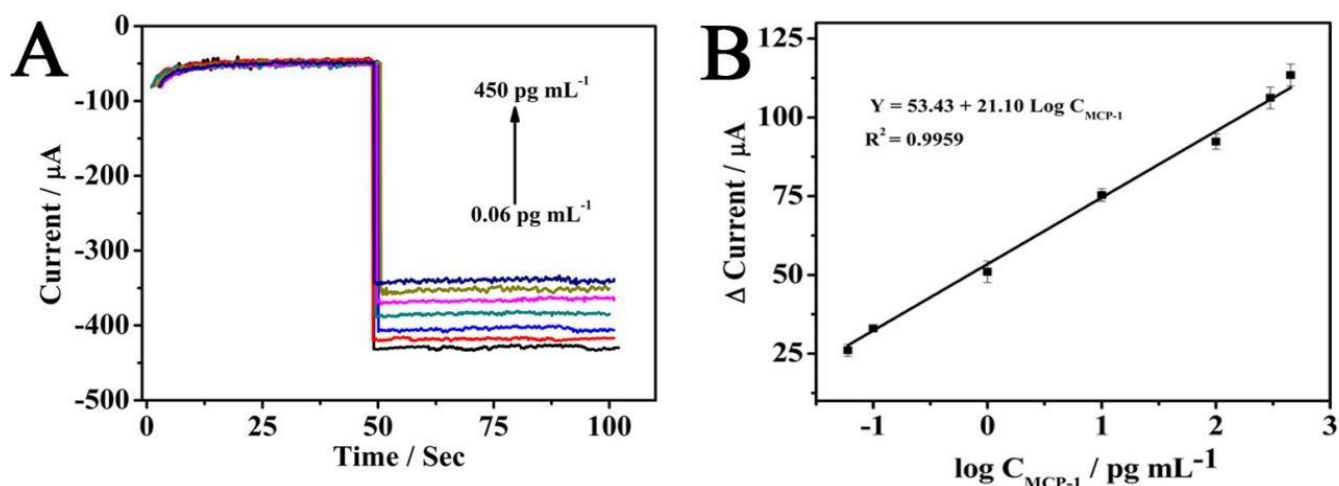


**Figure 6.** (A) Amperometric *i-t* curve response of the immunosensor for the detection of different concentrations of MCP-1: (a)  $0.06 \text{ pg mL}^{-1}$ ; (b)  $0.1 \text{ pg mL}^{-1}$ ; (c)  $1 \text{ pg mL}^{-1}$ ; (d)  $10 \text{ pg mL}^{-1}$ ; (e)  $100 \text{ pg mL}^{-1}$ ; (f)  $300 \text{ pg mL}^{-1}$ ; (g)  $450 \text{ pg mL}^{-1}$ . (B) Calibration curve of the immunosensor for different concentrations of MCP-1 ( $n=3$ ).

**Table 1.** Comparison of different methods for the detection of MCP-1

Method	Linear range (pg mL <sup>-1</sup> )	Detection limit (pg mL <sup>-1</sup> )	Reference
ELISA	31.2 - 2000	10	[36]
ELISA	15.6 - 1000	2.3	[37]
Electrochemical immunosensor	0.09 - 360	0.03	[38]
Electrochemical immunosensor	0.06 - 450	0.02	This work

### 3.5 Specificity, reproducibility and stability of the immunosensor

To evaluate the specificity, the proposed immunosensor was challenged with several interferences, such as ascorbic acid (AA, 0.5 ng mL<sup>-1</sup>), uric acid (UA, 0.5 ng mL<sup>-1</sup>), bovine serum albumin (BSA, 0.5 ng mL<sup>-1</sup>), L-cysteine (L-Cys, 0.5 ng mL<sup>-1</sup>) and glucose (Glu, 0.5 ng mL<sup>-1</sup>). As shown in Fig. 7A, the addition of 10 pg mL<sup>-1</sup> MCP-1 dramatically changed the electrocatalytic current response; however, other interfering substances did not induce obvious changes in the electrocatalytic current response. These results demonstrated that the fabricated immunosensor possessed excellent selectivity for MCP-1 detection.

Relative standard deviation (RSD) of intra-assay was used to evaluate the reproducibility of the immunosensor (Fig. 7B). Five electrodes were prepared for the detection of 10 pg mL<sup>-1</sup> MCP-1. As a result, the relative standard deviation (RSD) of the measurements was 2.44%, which suggested that the designed immunosensor had an acceptable reproducibility.

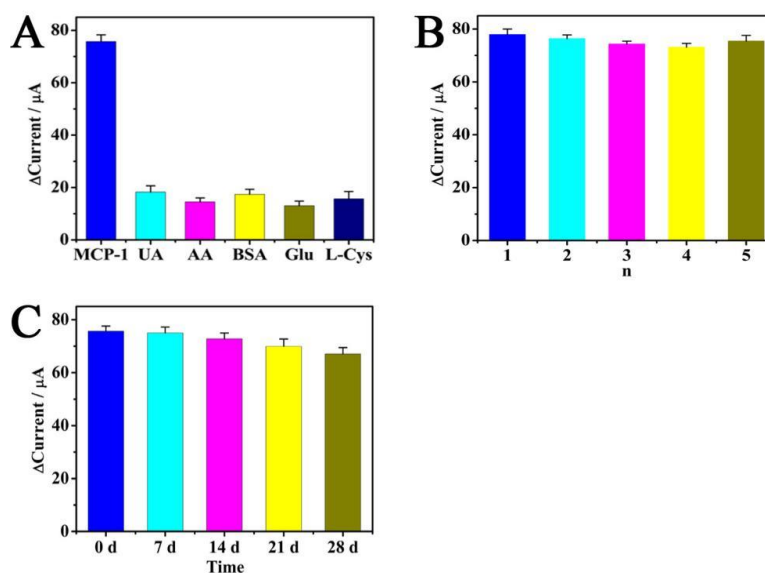


**Figure 7.** (A) The selectivity of the proposed immunosensor for the detection of MCP-1 (10 pg mL<sup>-1</sup>) against different interfering samples: uric acid (UA, 0.5 ng mL<sup>-1</sup>), ascorbic acid (AA, 0.5 ng mL<sup>-1</sup>), bovine serum albumin (BSA, 0.5 ng mL<sup>-1</sup>), glucose (Glu, 0.5 ng mL<sup>-1</sup>) and L-cysteine (L-Cys, 0.5 ng mL<sup>-1</sup>); (B) The electrocatalytic current responses of the prepared immunosensors were used to evaluate the reproducibility. Immunosensors 1 to 5 detected 10 pg mL<sup>-1</sup> MCP-1; (C) The stability of the prepared immunosensors with 10 pg mL<sup>-1</sup> MCP-1.

The stability of the immunosensor was explored over a period of 28 days of storage at 4 °C and measured every 7 days (Fig. 7C). The electrocatalytic current response of the immunosensor decreased gradually, and the last electrocatalytic current response retained 88.65 % of the initial electrocatalytic current response after 28 days, which indicated that the immunosensor had a good stability.

### 3.6 Analytical application of the immunosensor

To validate the feasibility of using the electrochemical immunosensor in clinical applications, a series of serum samples were analyzed by standard addition method. MCP-1 was diluted to 50, 100 and 200 pg mL<sup>-1</sup> with human serum, and the proposed immunosensor was used to detect different concentrations of MCP-1. As shown in Table 2, the recovery values ranged from 95.30% to 102.31% and the relative standard deviation values were in the range of 1.94% - 3.50%. We used ELISA to provide a quantitative comparison because the assay could precisely quantify the MCP-1 concentrations. The assay results of the immunosensor and ELISA showed an acceptable consistency, and the relative deviations were in the range of -5.50%—3.67%. These data clearly indicated that the immunosensor has promising applications in actual biological samples.

**Table 2.** Analysis data of the sensor for MCP-1 determination in human serum.

Serum samples (pg mL <sup>-1</sup> )	Immunosensor (pg mL <sup>-1</sup> )	RSD (%)	Recovery (%)	ELISA (pg mL <sup>-1</sup> )	Relative error (%)
50	47.65	3.50	95.30	50.41	-5.50
100	102.31	3.29	102.31	98.69	3.67
200	198.97	1.94	99.49	204.57	-2.74

## 4. CONCLUSIONS

In conclusion, a simple and efficient immunosensor for the rapid detection of MCP-1 based on PtNPs-SWCNHs was developed. The PtNPs-SWCNHs composite played an important role in the construction of the immunosensor, due to its large specific surface area, good biocompatibility, excellent conductivity and high catalytic activity. Under optimal conditions, the proposed immunosensor displayed superior analytical performances for the detection of MCP-1 with a low limit of detection, wide detection range, good selectivity, as well as acceptable reproducibility and stability. This immunosensor potentially could be applied for the determination of other biomarkers. However, further more investigations are needed before clinical applications.

## References

1. M.Y. Wu, C.J. Li, M.F. Hou, P.Y. Chu, *Int. J. Mol. Sci.*, 18 (2017) 2034.

2. X.L. Liu, P.F. Zhang, S.F. Ding, Y. Wang, M. Zhang, Y.X. Zhao, M. Ni, Y. Zhang, *PLoS One*, 7 (2012) e33497
3. B.J. Rollins, *Mol. Med. Today*, 2 (1996) 198.
4. S. Kitamoto, K. Egashira, *J. Atheroscler. Thromb.*, 9 (2002) 261.
5. S. Yla-Herttuala, B.A. Lipton, M.E. Rosenfeld, T. Sarkioja, T. Yoshimura, E.J. Leonard, J.L. Witztum, D. Steinberg, *Proc. Natl. Acad. Sci. USA*, 88 (1991) 5252.
6. O. Satiroglu, H.A. Uydu, A. Demir, M. Bostan, M. Atak, E. Bozkurt, *Tohoku J. Exp. Med.*, 224 (2011) 301.
7. S. Centi, S. Laschi, M. Mascini, *Bioanalysis*, 1 (2009) 1271.
8. P. Capaldo, S.R. Alfarano, L. Ianeselli, S.D. Zilio, A. Bosco, P. Parisse, L. Casalis, *ACS Sens.*, 1 (2016) 1003.
9. S. Su, M. Zou, H. Zhao, C.F. Yuan, Y.N. Xu, C. Zhang, L.H. Wang, C.H. Fan, L.H. Wang, *Nanoscale*, 7 (2015) 19129.
10. J. Shi, T.G. Cha, J.C. Claussen, A.R. Diggs, J.H. Choi, D.M. Porterfield, *Analyst*, 136 (2011) 4916.
11. Y.H. Wu, X.Y. Mao, X.J. Cui, L.D. Zhu, *Sens. Actuators, B*, 145 (2010) 749.
12. F. Cui, X.L. Zhang, *J. Electroanal. Chem.*, 669 (2012) 35.
13. X.Q. Lu, Y.Y. Li, J. Du, X.B. Zhou, Z.H. Xue, X.H. Liu, Z.H. Wang, *Electrochim. Acta*, 56 (2011) 7261.
14. N. Li, Z.Y. Wang, K.K. Zhao, Z.J. Shi, Z.N. Gu, S.K. Xu, *Carbon*, 48 (2010) 1580.
15. S.Y. Zhu, G.B. Xu, *Nanoscale*, 2 (2010) 2538.
16. S.A. Chechetka, M.F. Zhang, M. Yudasaka, E. Miyako, *Carbon*, 97 (2016) 45.
17. E. Bekyarova, K. Murata, M. Yudasaka, D. Kasuya, S. Iijima, H. Tanaka, H. Kahoh, K. Kaneko, *J. Phys. Chem. B*, 107 (2003) 4681.
18. T. Yoshitake, Y. Shimakawa, S. Kuroshima, H. Kimura, T. Ichihashi, Y. Kubo, D. Kasuya, K. Takahashi, F. Kokai, M. Yudasaka, S. Iijima, *Physica B*, 323 (2002) 124.
19. X.Q. Liu, L.H. Shi, W. X. Niu, H.J. Li, G.B. Xu, *Biosens. Bioelectron.*, 23 (2008) 1887.
20. F. Valentini, E. Ciambella, V. Conte, L. Sabatini, N. Ditaranto, F. Cataldo, G. Palleschi, M. Bonchio, F. Giacalone, Z. Syrgiannis, M. Prato, *Biosens. Bioelectron.*, 59 (2014) 94.
21. S.K. Arya, A. Dey, S. Bhansali, *Biosens. Bioelectron.*, 28 (2011) 166.
22. J. Zhao, L.M. Wei, C.H. Peng, Y.J. Su, Z. Yang, L.Y. Zhang, H. Wei, Y.F. Zhang, *Biosens. Bioelectron.*, 47 (2013) 86.
23. Z.Y. Yang, C.C. Qi, X.H. Zheng, J.B. Zheng, *Talanta*, 140 (2015) 198.
24. Z.G. Liu, Y.J. Guo, C. Dong, *Talanta*, 137 (2015) 87.
25. W.P. Deng, F. Liu, S.G. Ge, J.H. Yu, M. Yan, X.R. Song, *Analyst*, 139 (2014) 1713.
26. Y.C. Wei, X.J. Li, X. Sun, H.M. Ma, Y. Zhang, Q. Wei, *Biosens Bioelectron.*, 94 (2017) 141.
27. M. Giovanni, H.L. Poh, A. Ambrosi, G.J. Zhao, Z. Sofer, F. Sanek, B. Khezri, R.D. Webster, M. Pumera, *Nanoscale*, 4 (2012) 5002.
28. E. Bekyarova, A. Hashimoto, M. Yudasaka, Y. Hattori, K. Murata, H. Kanoh, D. Kasuya, S. Iijima, K. Kaneko, *J. Phys. Chem. B.*, 109 (2005) 3711.
29. Y.T. Liu, H.J. Wang, C.Y. Xiong, Y.Q. Chai, R. Yuan, *Biosens. Bioelectron.*, 87 (2017) 779.
30. L. Zhang, J.P. Lei, J. Zhang, L. Ding, H.X. Ju, *Analyst*, 137 (2012) 3126.
31. L. Yang, X. Ran, L. Cai, Y.C. Li, H. Zhao, C.P. Li, *Biosens. Bioelectron.*, 83 (2016) 347.
32. Y.Z. Niu, J.L. He, Y.L. Li, Y.L. Zhao, C.Y. Xia, G.L. Yuan, L. Zhang, Y.C. Zhang, C. Yu, *Microchim. Acta*, 183 (2016) 2337.
33. W.W. Huang, G.M. Xiang, D.N. Jiang, L.L. Liu, C. Liu, F. Liu, X.Y. Pu, *Electroanalysis*, 28 (2016) 1126.
34. G.L. Yuan, C. Yu, C.Y. Xia, L.L. Gao, W.L. Xu, W.J. Li, J.L. He, *Biosens. Bioelectron.*, 72 (2015) 237.
35. Y.C. Wei, X.J. Li, X. Sun, H.M. Ma, Y. Zhang, Q. Wei, *Biosens. Bioelectron.*, 94 (2017) 141.
36. R&Dsystems, Human ccl2/mcp-1 quantikine elisa kit, 2015.

37. ThermoScientific, Human mcp-1 elisa kits, 2015.

38. Y.L. Li, J.L. He, C.Y. Xia, L.L. Gao, C. Yu, *Biosens. Bioelectron.*, 70 (2015) 392.

© 2018 The Authors. Published by ESG ([www.electrochemsci.org](http://www.electrochemsci.org)). This article is an open access article distributed under the terms and conditions of the Creative Commons Attribution license (<http://creativecommons.org/licenses/by/4.0/>).